Doppler boosting effects on the radiation of relativistic jets

Gabriel Torralba Paz
Facultat de Física, Universitat de Barcelona, Diagonal 645, 08028 Barcelona, Spain.

Advisor: Valentí Bosch Ramon
(Dated: June 9, 2019)

Abstract: The geometry of high-mass microquasar jets is determined by the ram pressure of the stellar wind of the central star, which bends the jet outwards, and the orbital motion of the compact objects producing the jets. This structure emits radiation which is affected by the Doppler boosting effect.
Our goal is to understand how the wind determines the jet geometry and compute the effect of Doppler boosting on the luminosity.
To do this we use a simple model to compute the geometry, which is based on accounting for the wind-jet momentum transfer in the companion star non-inertial frame of reference.
The final geometry has an helical shape which gets larger with the distance to the jet base. Then, we study the luminosity for a full orbital phase of the jet for 3 different orbital inclinations. The results indicate changes in the luminosity due to Doppler boosting by about a 320-630% depending on the inclination.

I. INTRODUCTION

In a high-mass microquasar (HMMQ) there are two jets made of particles such as protons, electrons, positrons, etc., which flow in opposite directions. The jets come from a compact object which can be for example a neutron star or a black hole, orbiting a massive central star. The star expels a great amount of matter as a strong wind which pushes the jet outwards in the radial direction. If a non-inertial frame of reference is taken centered at the compact object a Coriolis force appears that pushes the jet in the counter-azimuthal direction. The resulting geometry of the jet is an helical shape that gets bigger as the flow goes farther[1,2]. To first order, this geometry is stationary and emits radiation which can be observed with a telescope on Earth. Since the jets have speeds close to the speed of light, they are affected by the Doppler boosting effect[3]. This relates the emitted and the observed luminosity by a factor which depends on the speed and the angle between the velocity of the emitter and the direction of the observer.
In this work we create a simple model for a high-mass microquasar using realistic parameters to see how it behaves after doing some assumptions. First we compute the geometry of the jet in the compact object frame of reference and compare the bending of the jet with respect to the vertical direction with the approximation found theoretically[2] called bending angle. Then we compute the total luminosity applying Doppler boosting. This is done for a full orbit and for different system inclinations. At the end we discuss the results and explain them.

II. DYNAMICS AND GEOMETRY OF THE JET

Our model consists on a compact object from which a jet is launched, orbiting a massive central star with a strong stellar wind. Since the two jets are very similar but move in opposite directions we suppose that they are not related and work with just one of them. To ease the calculations we will work in a cylindrical coordinate system (r, ϕ, z). The parameters used can be found in table I. Some assumptions have been made to simplify our problem: First of all we assume a circular orbit for simplicity. A circular motion approximation is enough at this stage for a high-mass microquasar. The jet will have an initial speed perpendicular to the orbital plane. We assume this speed is constant so when the stellar wind pushes it the direction of the velocity will change, but not its norm. We also assume that the jet has a conical shape that can be decomposed into small cylinders with a given height corresponding to the distance made by the jet in a differential of time dt and a radius r which increases as the jet goes farther with a height z

Parameter	Symbol	Value
Wind speed	$v_{\rm S}$	$2 \cdot 10^8$ cm s^{-1}
Wind mass loss rate	$\dot{M}_{\rm S}$	10^{-6} M$_\odot$ yr^{-1}
Jet luminosity	$L_{\rm J}$	10^{37} erg s^{-1}
Jet Lorentz factor	γ	2
Half-opening angle	$\theta_{\rm J}$	0.1 rad
Orbit radius	d_0	$3 \cdot 10^{12}$ cm
Period	T	4 d
Initial jet radius	r_0	$3 \cdot 10^{10}$ cm

TABLE I: Parameters used in this work.

$$dz = v_{\rm J} dt, \quad r_{\rm J} = \tan(\theta_{\rm J}) z_{\rm J}. \tag{1}$$

The jet has a rather compact structure, which is the part we can model, but after a turn of the helical structure the jet becomes unstable and the geometry gets disrupted[2]. We assume that in the region of the jet we model the fluid keeps laminar.

A. 2D Dynamics

Let us first study the jet dynamics in the star-compact object plane perpendicular to the orbital plane. The jet has a momentum rate[2] of:

$$\dot{P}_{\rm J} = \frac{L_{\rm J}}{c}\frac{\gamma_{\rm J}\beta_{\rm J}}{(\gamma_{\rm J}-1)}, \tag{2}$$

where $\beta_J = v_{\rm J}/c$. Then the momentum of a small cylinder at a certain time is $dP_{\rm J} = \dot{P}_{\rm J}\cdot dt$.
The stellar wind flows with a momentum rate of $\dot{P}_{\rm S} = \dot{M}_{\rm S}v_{\rm S}$ radially towards the jet and impacts the surface of each one of the small cylinders at a distance d_0. The wind hits it with an angle α between the wind direction and the velocity of the jet. The radial wind transfer momentum to the jet segment through the surface projected by the latter on the radial direction. The effective momentum rate of the stellar wind impinging on the segment is:

$$\dot{P}_{\rm S} = \dot{M}_{\rm S}v_{\rm S}\frac{2r_{\rm J}dz}{4\pi d^2}\sin\alpha, \tag{3}$$

where $2r_{\rm J}dz\sin\alpha$ is the effective surface, $r_{\rm J}$ is the radius of the corresponding cylinder and $d = \sqrt{r^2+z^2}$ is the distance from the central star to the segment.
This will be added to the momentum of the jet changing its direction. As said before, the stellar momentum rate does not modify the norm of the momentum of the jet but its direction, therefore the resulting momentum is normalized to the initial momentum $P_{\rm J}$. The jet changes its direction until $\alpha = 0$ corresponding to a momentum in the same direction as the stellar wind. The final inclination with respect to the z-axis can then be computed and compared to the theoretical bending angle[2].

B. 3D Dynamics

In the compact object frame of reference, which is non-inertial, a Coriolis force exists that drags the jet along the azimuthal direction in the opposite direction to the movement of the object. This force comes from the wind impacting the jet perpendicularly to the radial stellar wind and depends on the density $\rho_{\rm S}$ of the wind at every point[4]:

$$\rho_{\rm S} = \frac{\dot{M}_{\rm S}}{4\pi d^2 v_{\rm S}}, \tag{4}$$

where $v_{\rm S}$ is the stellar wind.
This force hits the jet surface projected in the azimuthal direction, where ψ is the angle between the jet direction and the counter-azimuthal direction. Now we can get the perpendicular force[4]:

$$F_\perp = \begin{cases} \rho_{\rm S}\left(\frac{4\pi}{T}\right)^2(r-d_0)^2 2r_{\rm J}dz\sin\phi & if \quad r < 2d_0 \\ \rho_{\rm S}\left(\frac{2\pi}{T}\right)^2 r^2\cdot 2r_{\rm J}dz\sin\phi & if \quad r > 2d_0 \end{cases} \tag{5}$$

where $2r_{\rm J}dz\sin\phi$ is the effective surface, similar to the 2D case. The previous equation is derived as follows: The perpendicular force can be approximated as $P_\perp \approx \rho_{\rm S}v_\perp^2$ [4]. In the non-inertial frame of reference, which corresponds to the compact object, a Coriolis force appears and accelerates the stellar wind in the perpendicular direction with an acceleration of $a_\perp = 2\Omega v_{\rm S}$ and a speed of $v_\perp = a_\perp\cdot t$. From here we get the first expression of equation 5. But there is a point when the perpendicular speed is greater than the compact object tangent velocity projected at larger radii $v_r = \Omega\cdot r$ and the stellar wind cannot go faster than v_r in the counter-azimuthal direction. This can be seen in the second expression where $\Omega = \frac{2\pi}{T}$ and this transition happens at $r = 2d_0$. As the jet goes farther, approximately after one turn, instabilities appear within the binary system and inside the jet causing the jet to break apart the conical shape and the jet model does not apply any more[2].

III. RADIATIVE CONSEQUENCES ON THE GEOMETRY

The geometry of the jet is stationary. It produces radiation through different mechanisms for different wavelengths such as inverse Compton scattering or synchrotron radiation. The intensity produced by the source, in our case the jet moving at constant speed, is modified due to relativistic effects[5]:

$$I_{observed} = u^3 I_{source}, \tag{6}$$

where $u = \gamma(1+\beta_{\rm J}\cos\theta_s)$, γ is the Lorentz factor and θ_s is measured in the emitting flow frame of reference. In our case the measured angle corresponds to the observed frame of reference θ_{obs} which is different than θ_s because of relativistic aberration[6]:

$$\cos\theta_s = \frac{\cos\theta_{obs}-\beta}{1-\beta\cos\theta_{obs}}. \tag{7}$$

The equation 6 will change to:

$$I_{observed} = \delta^3 I_{source}, \quad \delta = \frac{1}{\gamma(1-\beta_{\rm J}\cos\theta_{obs})}. \tag{8}$$

Using this we can get the luminosity[7] that we will study:

$$L_{obs} = \frac{\delta^3}{\gamma}L_{source}. \tag{9}$$

Our jet model is made of segments, each one of them has its own velocity, so for a given direction the angle θ_{obs} will vary as we go along all the structure. Since the observer is far away, the direction to the observer is the same for every piece of jet. The total luminosity will be the sum for each piece of the jet for a given orbital phase. From our point of view, the observer is at rest and the compact object is the one orbiting the central star, but if we move to the compact object non-inertial frame of

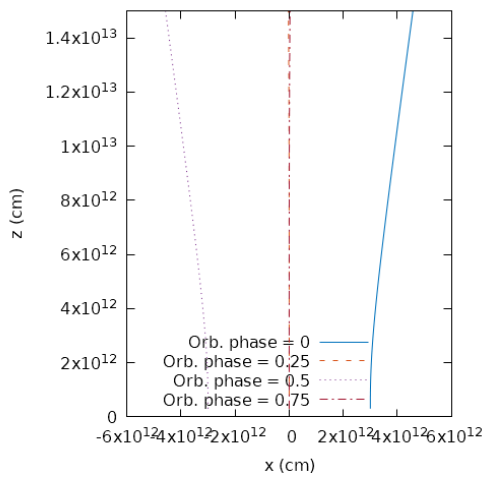

FIG. 1: Structure of the jet in the x-z plane for different orbital phases. Notice that the jet bends in the y direction for orbital phases 0.25 and 0.75, that is why it appears as a straight line.

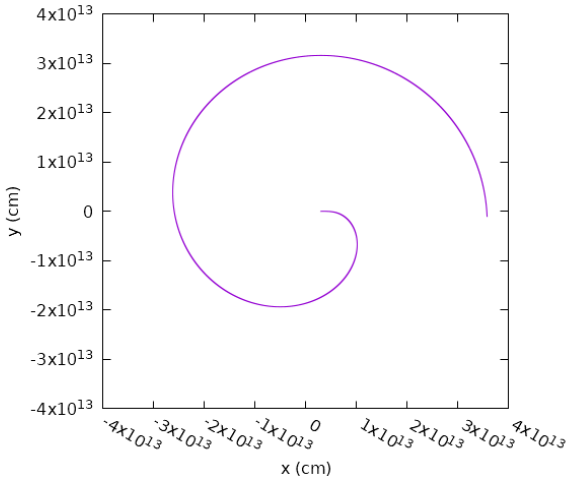

FIG. 2: Structure of the jet for the x-y plane.

reference now the observer will be the one orbiting the central star. So it is easier to make the observer move to a constant angular speed corresponding to a period of the microquasar $\omega = 2\pi/T$ since we have the geometry of the jet in this same frame of reference.

IV. RESULTS

Using the parameters found at table I we obtain the following results. If we suppose no orbital movement and using equations 2 and 3 we see that the jet bends outwards as seen in figure 1. Notice that the ram pressure of the stellar wind compared to that of the jet is small and the bending angle is small, too. The corresponding jet bending angle with respect to the vertical direction can be compared to the theoretical bending angle[2]. The equations from [2] are an approximation to the model we are using, therefore the result will not match really well but with an error of 10%. Using our parameters, the bending angle gives 7.8°, while the angle computed using our model gives 7.5°. If we compute the relation between both we see that they differ in 4%, so we can say that our numerical model until now matches the analytic theory.
After applying the orbital movement, the jet evolves forming an helical pattern which combined with the radial movement gives an helix which gets bigger the farther the flow goes (figures 2 and 3). To see the pattern we transform the coordinates into a Cartesian coordinate system. As said before, the jet becomes unstable after a turn so an extrapolation of our model will lead us to wrong results. Initially, the jet begins to bend like the 2D case. This happens because the radial stellar wind is stronger at smaller distances compared to the Coriolis force. When the radial wind becomes weaker, the perpendicular force becomes noticeable and turns the jet

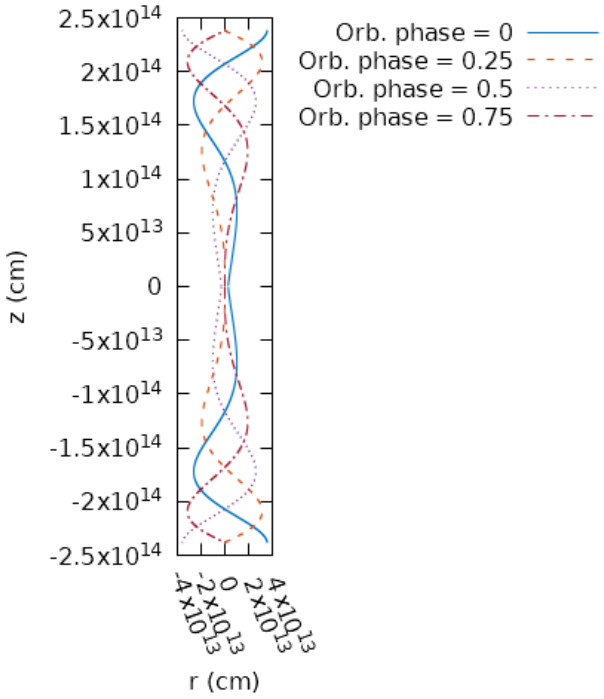

FIG. 3: Structure of both jets in the x-z plane for different orbital phases. This is a zoom-out of figure 1

doing the helical pattern. To see this effect we could extrapolate the model and see that the radius of the jet increases more slowly and the spiral in figure 2 would be more and more squished since the radial component of the velocity decreases.
After we have the results of the jet geometry we can compute the luminosity. In figure 4a and 4b we plot the variation of the angle for different orbital phases. For greater angle θ_{obs} the Doppler factor will be lower since the jet is pointing less towards us. In figure 4c and 4d we represent the Doppler factor for two different inclinations.

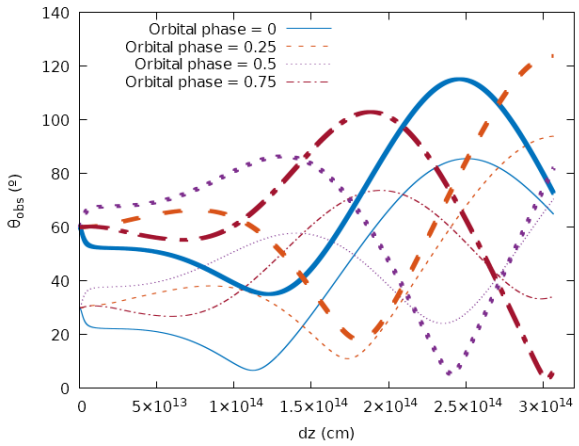

(a) Angle between the velocity of the emitter and the direction of the observer of the jet for inclinations of 30 (thin line) and 60 (thick line) degrees.

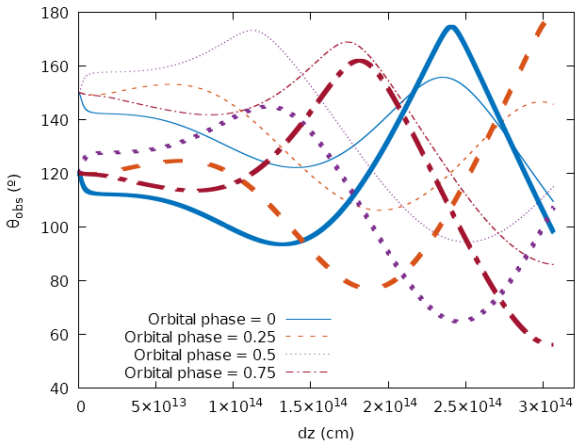

(b) Angle between the velocity of the emitter and the direction of the observer of the counter-jet for inclinations of 30 (thin line) and 60 (thick line) degrees.

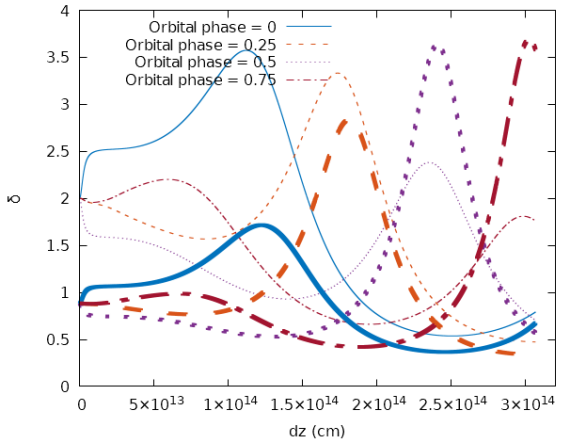

(c) Doppler factor with distance along the jet for inclinations of 30 (thin line) and 60 (thick line) degrees.

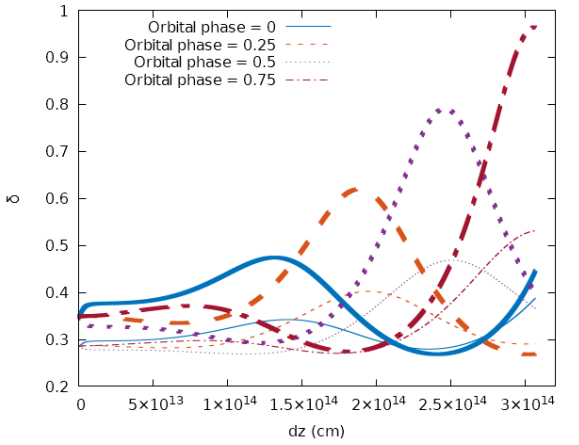

(d) Doppler factor with distance along the counter-jet for inclinations of 30 (thin line) and 60 (thick line) degrees.

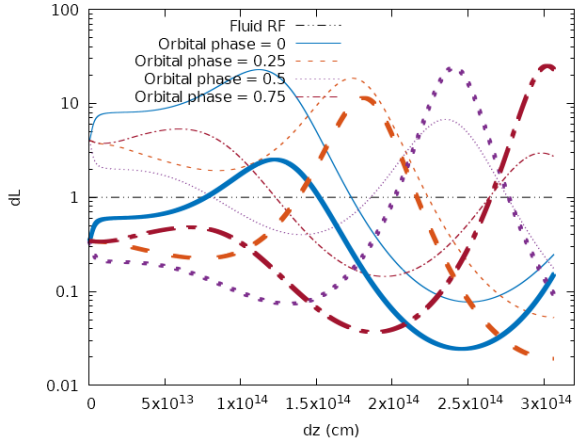

(e) Luminosity per segment of the jet for inclinations of 30 (thin line) and 60 (thick line) degrees.

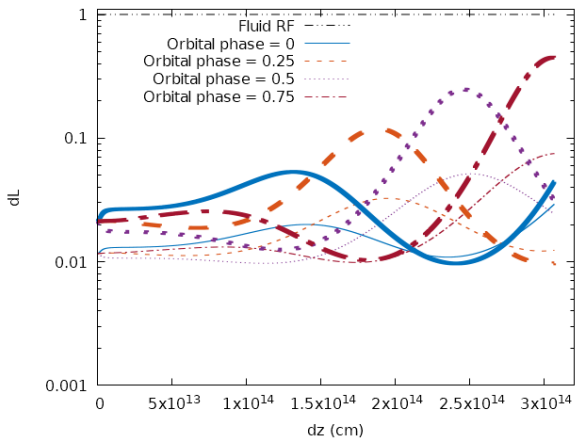

(f) Luminosity per segment of the counter-jet for inclinations of 30 (thin line) and 60 (thick line) degrees.

FIG. 4: Data corresponding to the jet (left) and the counter-jet (right).

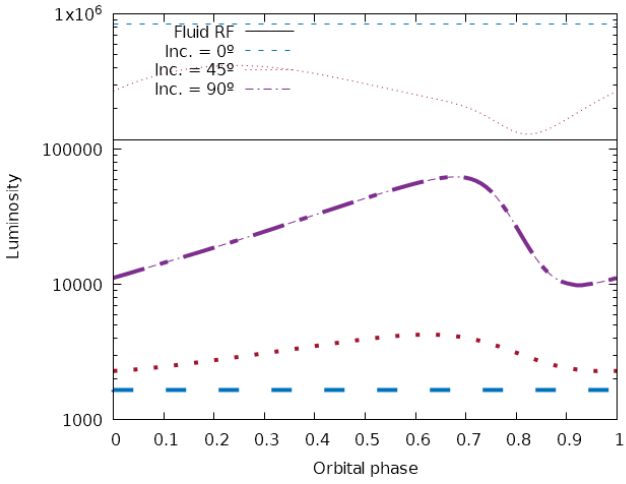

FIG. 5: Luminosity for the jet (thin line) and the counter-jet (thick line) and different inclinations. Notice the difference between the jet and the counter-jet.

When the jet begins to bend in the counter-azimuthal direction the Doppler factor increases until it arrives to a maximum when the cosine of the angle θ_{obs} is maximum as seen in equation 8. After that the Doppler factor decreases, but can have another peak, depending on the orbital phase. Notice that the Doppler factor for the jet is greater than the one for the counter-jet, which makes sense since the jet usually goes in the opposite direction to the observer, with angles greater than 90 degrees, making the Doppler factor small. The same happens in figure 4e and 4f, where the peaks are in the same position as expected, but the difference is even more remarkable. Notice that the counter-jet begins to have greater luminosity per segment as it goes farther, since the velocity along the z-axis decreases and the angle θ_{obs} becomes usually smaller. In figure 5 we represent the variation of the total luminosity for 3 different inclinations and a luminosity per cylinder of 1. This has been done to simplify the computation since the final number is not important, but the variation of the luminosity. As expected, at an orbital phase of 0 and 1 the luminosity is exactly the same, which tells us that the observer completed a full turn. For an inclination of 0° we see the jet as in figure 2, which means that we see the same structure for a full orbital phase, therefore the luminosity observed is constant. For the counter-jet the luminosity is much lower than the luminosity from the jet, thus we can neglect the counter-jet in this case. For inclinations greater than 0° the curve begins to have an important variation, and the luminosity of the counter-jet is still negligible. But for an angle of 90°, corresponding to the orbital plane, we would see the jet and the counter-jet as in figure 3. The luminosity in this case is the same for both jets since they are the reflection of the other jet. If the micro quasar is not pointing towards us we will see a variation of the luminosity by 320-630%, depending on the inclination.

V. CONCLUSIONS

Using a simple model we describe the geometry and the effect of Doppler boosting on the emission of the jets of high-mass microquasars. We find that the luminosity may change by 320-630% along the orbit, depending on the inclination. Interestingly, because of the strong deviation of the jet on large scales, the Doppler boosting effect becomes stronger when the inclination is larger, unlike the case of straight jets.

Acknowledgments

I would like to thank my advisor Valentí Bosch Ramon for guiding me and helping me with some issues during the development of this work.

[1] V. Bosch-Ramon. The innermost regions of relativistic jets and their magnetic fields. *European Physical Journal Web of Conferences*, 61(03001), 2013.
[2] M. V. Bosch-Ramon, V. & Barkov. The effects of the stellar wind and orbital motion on the jets of high-mass microquasars. *A&A*, 590(A119), 2016.
[3] Bosch-Ramon V. & Uchiyama Y. Khangulyan, D. Inverse compton emission from relativistic jets in binary systems. *MNRAS*, 481(2):1455–1468, 2018.
[4] M. V. Bosch-Ramon, V. & Barkov. Large-scale flow dynamics and radiation in pulsar γ-ray binaries. *A&A*, 535 (A20), 2011.
[5] M. & Teller E. Johnson. Intensity changes in the doppler effect. *PNAS*, 79:1340, 1982.
[6] A Einstein. Zur elektrodynamik bewegter krper. *Annalen der Physik*, 322(10):891921, 1905.
[7] Madejski G. Moderski R. & Poutanen J. Sikora, M. Learning about active galactic nucleus jets from spectral properties of blazars. *ApJ*, 484(108-117), 1997.